Synthesis and physical properties of the ferroelectromagnetic composites $(1 - x)\text{PbMn}_{1/3}\text{Ta}_{2/3}\text{O}_3 - x\text{PbTiO}_3$

Kamaludin Abdulvakhidov[1] · Alexander Soldatov[1] · Bashir Abdulvakhidov[2] · Sadyk Sadykov[2] · Ivan Dmitrenko[1] · Zhengyou Li[1] · Alexander Nazarenko[3] · Marina Sirota[4] · Marina Vitchenko[4]

Abstract

In this paper, we present the synthesis and studies of physical properties of the ferroelectromagnetic composites $(1–x)$ $\text{PbMn}_{1/3}\text{Ta}_{2/3}\text{O}_3–x\text{PbTiO}_3$ $[(1–x)\text{PMnT}–x\text{PT}]$, which exhibit a relaxor behavior. Using a synergistic application of scanning electron microscopy (SEM), X-ray structure analysis, and energy-dispersive X-ray analysis (EDX), we revealed that two phases always coexist in the synthesis of the composition $\text{PbMn}_{1/3}\text{Ta}_{2/3}\text{O}_3$ (PMnT), one phase of which has a pyrochlore structure, and the other has a pseudo-cubic cell of the perovskite structure. We further demonstrated that doping with lead titanate PbTiO_3 (PT) suppresses the dielectric polarization's relaxor behavior. Using X-ray diffraction techniques at room temperature, we studied the dependencies of the structural parameters of each phase on the mole fractions of PT. The dielectric characteristics were studied at various frequencies by the dielectric spectroscopy method, and the dependency of the bandgap E_g on the dopant's mole fractions was determined by the optical absorption method. The dopant's influence on the IR Fourier spectra and magnetic hysteresis loops was analyzed. The magnetodielectric and magnetoresistive effects in these composites were studied.

Keywords Multiferroic composite · Perovskite · Pyrochlore · Magnetoresistance · Dielectric loss

1 Introduction

In recent years, ferroelectrics with spontaneous magnetization have attracted significant interest from researchers, since magnetic and ferroelectric subsystems' mutual influence forms a number of exciting effects in these composites. In scientific papers, such materials are usually called multiferroics, which are characterized by the presence of at least two of the three types of orders: magnetic, electrical, and mechanical [1]. Compared to the single-phase multiferroics, multiferroic composites exhibit much higher magnetoelectric (ME) coupling. It becomes a promising candidate for magnetic field sensors and next-generation low-power memory devices [2]. The coexistence of spontaneous magnetic moments and polarization does not contradict the general criteria for ferromagnetism and ferroelectricity. Magnetic ordering is determined by the exchange interaction of electron spins, and ferroelectric ordering is determined by the redistribution of the charge density in the lattice.

It is well known that the electrical and magnetic subsystems of crystals are most sensitive near the boundaries of ordered and disordered phases. However, until now, multiferroics have not received a wide practical application due to the weakness of the correlated magnetic and electric effects, and the large interval between the temperatures of the ferroelectric and ferromagnetic phase transitions. Nevertheless, the current research for new complex composites and various modifications of already known composites also yield exciting results. The main requirements for the composites to have multiferroic properties are the presence of at least one of 3d-elements (Tl, B, Fe, Mn, Cr, Ni) responsible for magnetic properties, and at least one of Pb, Bi, Ba, Zr, Nb, W elements that have high polarizability

✉ Kamaludin Abdulvakhidov
   phys.kam@mail.ru

1   The Smart Materials Research Institute, Southern Federal University, Sladkova 178/24, Rostov-on-Don, Russia 344090

2   Dagestan State University, Gadgieva 43-a, Makhachkala, Russia 367000

3   Southern Scientific Center of the Russian Academy of Sciences, Chekhova 41, Rostov-on-Don, Russia 344006

4   Don State Technical University, Gagarina 1, Rostov-on-Don, Russia 344000

are responsible for ferroelectric properties. Furthermore, a giant magnetoresistance was observed in $Tl_2Mn_2O_7$, which has a pyrochlore structure and thus differs both structurally and electronically from perovskites [3].

The results of studying the structural parameters and physical properties of the ferroelectromagnetic multiferroic $(1-x)PbMn_{1/3}Nb_{2/3}O_3-xPbTiO_3$ were published previously, which exhibited a relaxor polarization behavior and was first obtained without an impurity phase [4]. It was found that $PbMn_{1/3}Nb_{2/3}O_3$ (PMnN) can mainly be obtained in a monophase state, and its dopant's mole fractions in the range of $1.5 \leq x \leq 2.5$ lead to the formation of a morphotropic phase transition region. As is known, ferro-piezoelectric composites from the morphotropic region have extreme properties (increased sensitivity to external factors and stability of properties in a wide range of external factors), which allows them to be classified as functional smart materials.

Earlier, in single-phase perovskite manganites, the colossal magnetoelectric effects were observed in the form of a ferroelectric phase transition induced by magnetic fields [5] and ferromagnetism induced by electric fields in hexagonal manganites [6].

Complex ferromagnetic manganese-containing ferroelectrics-multiferroics are of great interest from both theoretical and practical points of view. They can feature undoubtedly random fields caused by a disorder in interstices, lead and oxygen vacancies, ions of impurities, and dopants. The sources of random fields, which are randomly located electric dipoles, tend to order the system using indirect dipole–dipole interactions with a soft mode of the initial phase, while other sources of random fields tend to disorganize the system [7]. Taking these fields into account, we can observe anomalies in the nonlinear dielectric constant [8], which could be identified by the Vogel-Fulcher law [9], and the deviation of the dielectric constant's behavior can be described by Debye's law. The addition of the classical ferroelectric $PbTiO_3$ of various concentrations to relaxor multiferroics leads to the formation of a morphotropic phase transition region, which would bring a change in the vibrational spectrum of the crystal lattice, high values of dielectric permittivity, and variable electromechanical properties.

However, lead-containing composites are not always obtained in a monophase state. Very often, the formation of a perovskite phase is accompanied by the formation of a pyrochlore phase. Such composites have stable physical properties in a wide range of external influences. For example, they can be excellent materials for a capacitor.

This work aims to analyze the composition of multiphase formed during the synthesis of the composites $(1-x)PMnT-xPT$ and to study their physical properties.

2 Materials and methods

2.1 Synthesis

To prepare the PMnT composition, the corresponding stoichiometric amounts of Mn and Ta oxides ($MnO \geq 99.9\%$, $Ta_2O_5 \geq 99.9\%$) were mixed in a Pulverisette 7 planetary mill for 30 min at a rotational speed of 600 rpm. Then, the mixture was heated for 2 h at 900 °C. After that, the furnace was turned off and cooled by inertia to room temperature. The resulting composition was mixed with the stoichiometric amount of Pb oxides ($PbO \geq 99.9\%$) and ground in an agate mortar for 2 h in the presence of ethanol, then thermostat-dried at 100 °C to remove moisture. The dried composition was homogenized in the planetary mill for 30 min at a rotational speed of 800 rpm. In order to determine the optimal technological parameters, the resulting mixture was divided into seven portions and was heated in the temperature range 850–1150 °C with a step of 50 °C, for 2 h.

The solid-phase synthesis also prepared the doping composition of lead titanate (PT). The corresponding stoichiometric amounts of Pb and Ti oxides ($PbO \geq 99.9\%$, $TiO_2 \geq 99.9\%$) were mixed in an agate mortar for 2 h in the presence of ethanol. The resulting mixture was heated for 2 h at 1000 °C. X-ray phase analysis showed the absence of impurity phases and the tetragonal systems of the obtained PT.

For the joint synthesis $(1-x)PMnT-xPT$, eight different molar fractions ($x = 0.2, 0.3, 0.4, 0.5, 0.6, 0.7, 0.8,$ and 0.9) were taken, mixed, and had been being ground for 2 h in an agate mortar in the presence of ethanol. Sintering of ceramics $(1-x)PMnT-xPT$ took place at temperatures of 850, 900, 950, and 1000 °C for 2 h in order to determine the optimal technological parameters. The sintered ceramic samples had a diameter of 10 mm and a thickness of 1 mm. The conductive pads for electrodes were formed on both sides of ceramic disks by casting the silver paste and annealing it at 750 °C for 20 min in air.

2.2 Characterization

The study of these samples' microstructure was conducted by using a scanning electron microscope (Carl Zeiss EVO 40, Germany) at the Center for Collective Use of the State Research Center of the Russian Academy of Sciences (No. 501994). Elemental analysis was carried out using a special X-ray attachment for energy-dispersive analysis (INCA Energy). The density of ceramics was measured by the hydrostatic weighing method. These values were limited in the range of 6.7–7.1 g cm^{-3} and increase with

the increase in PT's mole fraction in $(1-x)$PMnT–xPT samples. The composites' phase analysis was carried out on an X-ray diffractometer (D2 Phaser), which uses Cu $K_{\alpha 1,2}$ radiation with the 2θ step of $0.01°$ and the acquisition time is 0.1 s per point. The temperature-dependence dielectric measurements were performed using the experimental setup with an E7-20 immittance meter manufactured by the Minsk Research Institute of Instrumentation. The Fourier-transform infrared (FTIR) spectra were recorded on an FSM-1202 (Infraspec, Russia) spectrometer with a resolution of 1 cm^{-1}. For IR measurements, the ceramics were ground into powder, then mixed with KBr in a mass ratio of 1:100 and then pressed into cylindrical disks with a diameter of 13 mm and 1 mm thick. Optical absorption spectra at room temperature were studied on a Shimadzu UV-2600 two-beam spectrophotometer. X-ray absorption near-edge structure (XANES) spectra were measured using a laboratory XAS instrument (Rigaku, R-XAS Looper) in transmission mode. The magnetic properties were studied using a vibrating sample magnetometer (LakeShore 7404).

3 Results and discussion

3.1 Composition and morphology

The study of the microstructure and elemental composition of the various cleavage regions of the undoped reference PMnT ceramic samples (using an electron microscope and an attachment "INCA Energy" for energy-dispersive analysis) showed that the ceramic grains differ in both crystal habit and elemental composition. Figure 1 shows a micrograph of one of these samples and an energy diagram corresponding to one of its crystallites. As it can be seen from the energy diagram (Fig. 1a′), at the studied point (in Fig. 1a it is indicated by a vertical arrow), Mn ions are not detected, and the crystallite itself has the shape of an octahedron,

which is characteristic of pyrochlore phases often found in perovskites.

At the same time, the study of a crystallite of a flatter shape (indicated by the horizontal arrow) showed Mn ions' presence. This principle has turned out to be typical for different points of all studied samples.

3.2 X-ray structural and spectral analysis

One of the typical diffraction patterns of PMnT synthesized at 1000 °C is presented in Fig. 2a, b shows the diffractogram of the composites 0.1PMnT–0.9PT. Diffraction patterns were processed by the full-profile Rietveld method using the software Powder Cell 2.3 [10].

The Pseudo–Voigt profile function was used to refine the lattice parameters. The pseudo-cubic (perovskite) phase with the unit cell parameter $a_{per} = 3.995 \pm 0.002$ Å and the pyrochlore phase with the unit cell parameter $a_{pyr} = 10.546 \pm 0.002$ Å. The Miller indices corresponding to these phases are shown in Fig. 2a, b in blue and red, respectively. The energy-dispersive analysis made it possible to identify the pyrochlore phase as a composition corresponding to the range of existence of $Pb_{1.94}Ta_2O_{6.94} - Pb_{1.96}Ta_2O_{6.96}$. The perovskite phase corresponds to the formula $Pb_{0.70}Mn_{0.306}Ta_{0.66}O_{2.96}$. As can be seen from these formulas, both the pyrochlore and perovskite phases are anion–cation deficient.

By comparing the XANES spectrum of $Pb_{0.70}Mn_{0.306}Ta_{0.66}O_{2.96}$ with the reference spectra of Mn_2O_3 and MnO_2, we found that Mn has a valence state of $+4$. Figure 3 shows these results.

Other researchers also reported a change in the Mn valence. For example, a change in the Mn valence (from $+4$ to $+3$) was revealed by the magnetic susceptibility measurements in the ferroelectric ceramic $Ba(Ti_{0.995}Mn_{0.005})O_3$-$xBiO_{3/2}$ (x = 0.001, 0.002, 0.003), which was obtained by conventional solid-state synthesis and sintering [11]. A change in the Mn valence [$Mn^{(4+)}O_2$ (873 K)$\rightarrow Mn_2^{(3+)}O_3$
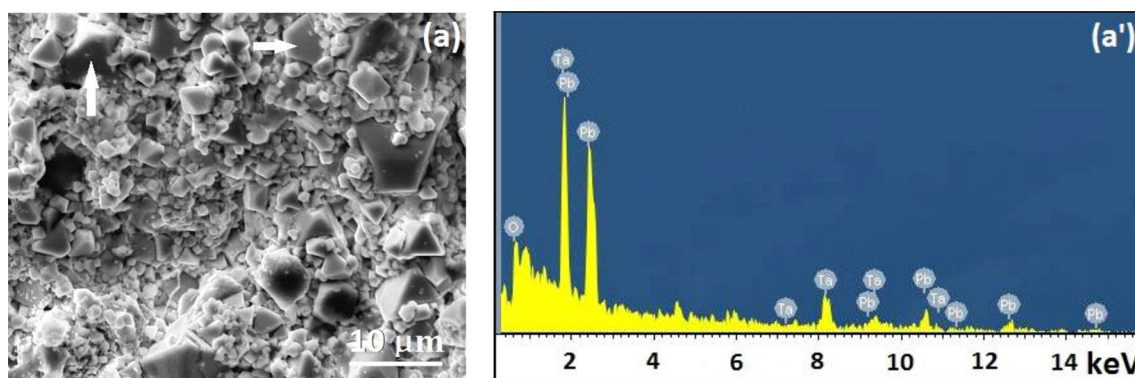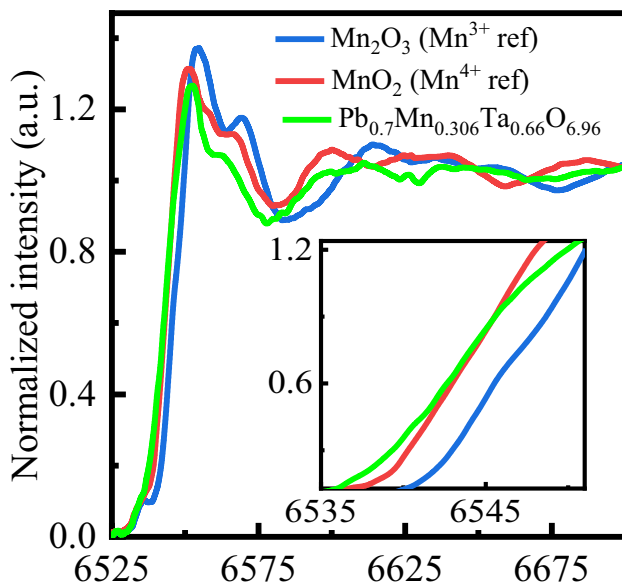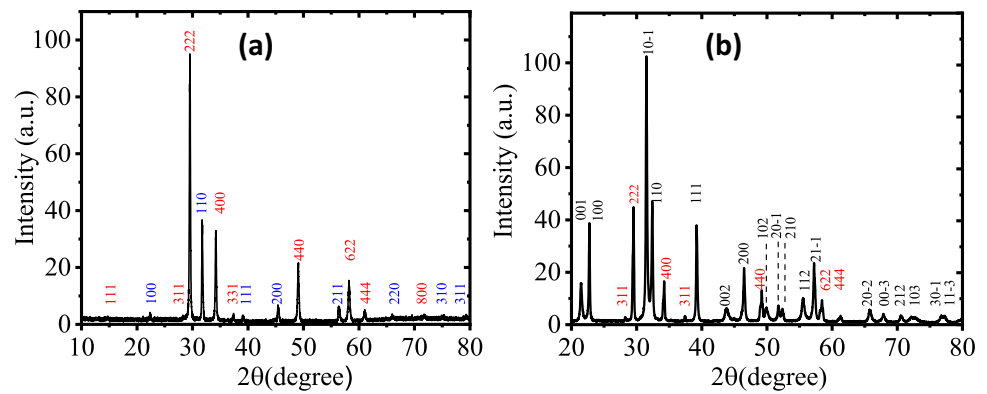

Fig. 1 The electron micrograph of PMnT (**a**) and its energy spectrum (**a′**) corresponding to the crystallite indicated by the vertical arrow

Fig. 2 Diffraction patterns of the composites PMnT (**a**) and 0.1PMnT–0.9PT (**b**)

Fig. 3 The Mn K-edge X-ray absorption near edge structure (XANES) spectra of Mn_2O_3, MnO_2, and $Pb_{0.70}Mn_{0.306}Ta_{0.66}O_{2.96}$

$(1173\ K) \rightarrow Mn_3^{(2+)+(3+)}O_4$ (1573 K)] was also observed in $YCu_xMn_{1-x}O_3$ ($x = 0.05, 0.10, 0.15$) ceramic solid solution during the synthesis and sintering [12]. In the $MnCO_3$ compound, Mn^{2+} was oxidized to Mn^{4+} fractionally in 1300 °C in air, and some Mn^{2+} were oxidized to Mn^{3+} [13].

At this stage, we were unable to establish the exact space group of symmetry of the perovskite phase; however, from $(h^2 + k^2 + l^2)$, it can be seen that the cell is primitive, P. The symmetry of the pyrochlore phase corresponds to the space group Fd3m. Earlier, a similar pyrochlore phase with the molecular formula $Pb_{1.5}Ta_2O_{6.5}$ was studied in [14]. It has been found that the composition has a defective pyrochlore structure without the ordering of oxygen and lead vacancies and without displacement of atoms from their centrally symmetric positions. The cell parameter calculated by the authors of that work [14] is $a = 10.555$ Å, which slightly differs from the parameter value obtained. The authors

interpreted the small but significant changes in the lattice parameters in that work [14] as a consequence of the existence of a composition range, which is estimated as $Pb_{1.3}Ta_2O_{6.3}$–$Pb_{1.5}Ta_2O_{6.5}$. Electrical measurements have shown that the compound has predominantly electronic conductivity, and the ionic contribution to total conductivity is very small, even at the highest temperatures used in the study.

In [15], not only rhombohedral and orthorhombic phases, but also a defective cubic pyrochlore phase with the same composition interval were observed in the synthesis of the PbO–Ta_2O_5 system, and it is shown that a stable pyrochlore phase corresponding to the formula $Pb_2Ta_2O_7$ was not formed.

Figure 4 shows the dependencies of the unit cell parameters of all $(1-x)$PMnT–xPT phases on the dopant PT's mole fraction. The pyrochlore phase parameter a_{pyr} decreases over the entire doping range, while the perovskite phase parameter a_{per} decreases in the PT's mole fractions range 0.2–0.6. Due to the low mole fractions of PT and the overlap of diffraction profiles, it was possible to record the Bragg peaks reliably and calculate the tetragonal cell parameters a_T and c_T of PT only for the mole fraction of PT at $x = 0.5$ and higher. For the same reason, to the left of $x = 0.5$, these parameters' behavior is still unknown. The interval of $x = 0.5 - 0.6$ is characterized by a sharp increase in c_T and the same sharp decrease in a_T. As can be seen from Fig. 4b, the half-width of the Bragg peak from the (222) plane of the pyrochlore phase, $FWHM_{(222)pyr}$, has a sharp jump when the mole fraction of PT at $x = 0.1$, and with a further increase in x, the half-width decreases from 0.29° to 0.14°.

In this case, the pyrochlore's phase concentration in the range $0 \leq x \leq 0.5$ also decreases, while the concentration of the perovskite (pseudo-cubic) phase increases. Further, at the point of $x = 0.6$, we observed a sharp increase in the pyrochlore phase's concentration by 30%; after that, the monotonic decreased. The mole fraction range $0.5 \leq x \leq 0.6$ is also notable because starting from $x = 0.5$, tetragonal splitting is distinguished, and at $x = 0.6$, a jump in the unit cell
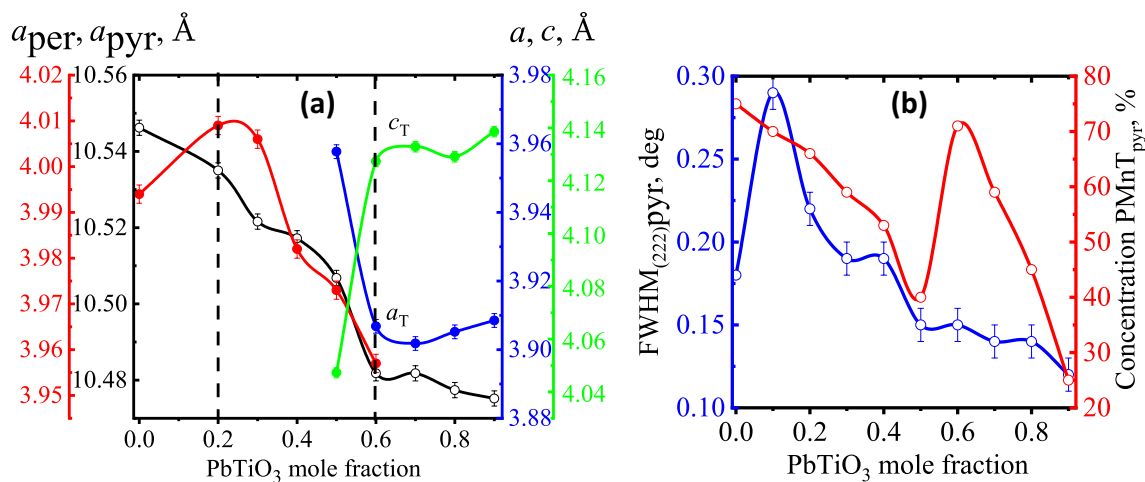
Fig. 4 **a** The calculated lattice parameters for perovskite, a_{per} (red), pyrochlore, a_{pyr} (black) and for tetragonal phases, a_T and c_T (blue and green, respectively), **b** FWHM$_{(222)}$, and concentration of pyrochlore phase $(1–x)$PMnT–xPT constructed as a function of x

parameters of this phase is observed. However, at $x \geq 0.6$, the diffraction peaks of the pseudo-cubic phase overlap with the tetragonal phase peaks, which, in turn, dominates and controls the pseudo-cubic phase's unit cell parameters. Consequently, the introduction of lead titanate into the composite PMnT leads to the relaxation of mechanical stresses in the pyrochlore phase and also leads to a decrease in the pyrochlore phase concentration and its unit cell parameters.

3.3 Dielectric properties

Earlier in [16], it was shown that the introduction of PT into PbMg$_{1/3}$Nb$_{2/3}$O$_3$ makes it possible to increase the degree of long-range ordering, and at high mole fractions of PT in ferroelectric solid solutions, there is a transition from the relaxor behavior of the dielectric constant to the behavior of classical ferroelectrics.

As a ferroelectric, PMnT belongs to the group of compounds with the general formula PbB$^{2+}_{1/3}$B$^{5+}_{2/3}$O$_3$, the typical representatives of which are PbMg$_{1/3}$Ta$_{2/3}$O$_3$ [17], PbMg$_{1/3}$Nb$_{2/3}$O$_3$, and other compounds [18]. These compounds' features are diffuse phase transition; a high dielectric constant ($\sim 10^3$); the formation of a perovskite phase through an intermediate pyrochlore phase; and dielectric constant's relaxor behavior in the phase transition region. Typical frequency-temperature dependencies of the real part of the dielectric constant ε' and the dielectric loss tgδ of the composite PMnT are shown in Fig. 5a, a′, respectively. As seen in Fig. 5a, the phase transition is smeared out, and ε' is characterized by a relaxor behavior.

A separate relaxor phase usually does not give a flat plateau at low frequencies in the $\varepsilon'(T)$ dependency; however, the pyrochlore phase's presence may smooth the phase transition of the perovskite phase to some extent. It is also possible that

this is the result of phase transitions between the perovskite and pyrochlore (but non-ferroelectric) phases. It is known that the high electronic polarizability of Pb ions can be the cause of phase transitions in lead-containing pyrochlores. This was pointed out earlier in [19]. The Curie–Weiss law is not valid for pyrochlores above the maximum permittivity temperature (T_m), and in the region of the low-temperature decay, the dielectric polarization has a relaxation character. Fig. 5b,b′ shows the dependencies of $\varepsilon'(T)$ and tg$\delta(T)$ corresponding to the composite 0.4PMnT–0.6PT. As it can be seen from the figures, with an increase in the mole fractions of the dopant PT, two anomalies are observed in the $\varepsilon'(T)$ dependency due to coexisting phases, and the tg$\delta(T)$ curves of this composite are characterized by a steeper rise than the tg$\delta(T)$ curves of composite PMnT.

An increase in the PT's mole fractions led to significant suppression of the first maximum, an increase in the second maximum on the $\varepsilon'(T)$ dependency, a relatively sharp increase in tg$\delta(T)$, and suppression of the relaxor behavior of ε'. As an example, Fig. 5c,c′ shows these plots of these dependencies for the composite 0.1PMnT–0.9PT.

3.4 Optical spectra

Optical absorption spectra of solids are one of the essential tools for studying their structural perfection. The bandgap (E_g) determined from these spectra is one of the most critical parameters, which are the inhomogeneities, structural defects, and crystal lattice impurities. To determine E_g, we focused on studying the intrinsic optical absorption. The absorption edge analysis makes it possible to establish the type of optical transition and determine E_g and its anomalies during phase transitions in ferroelectromagnets.
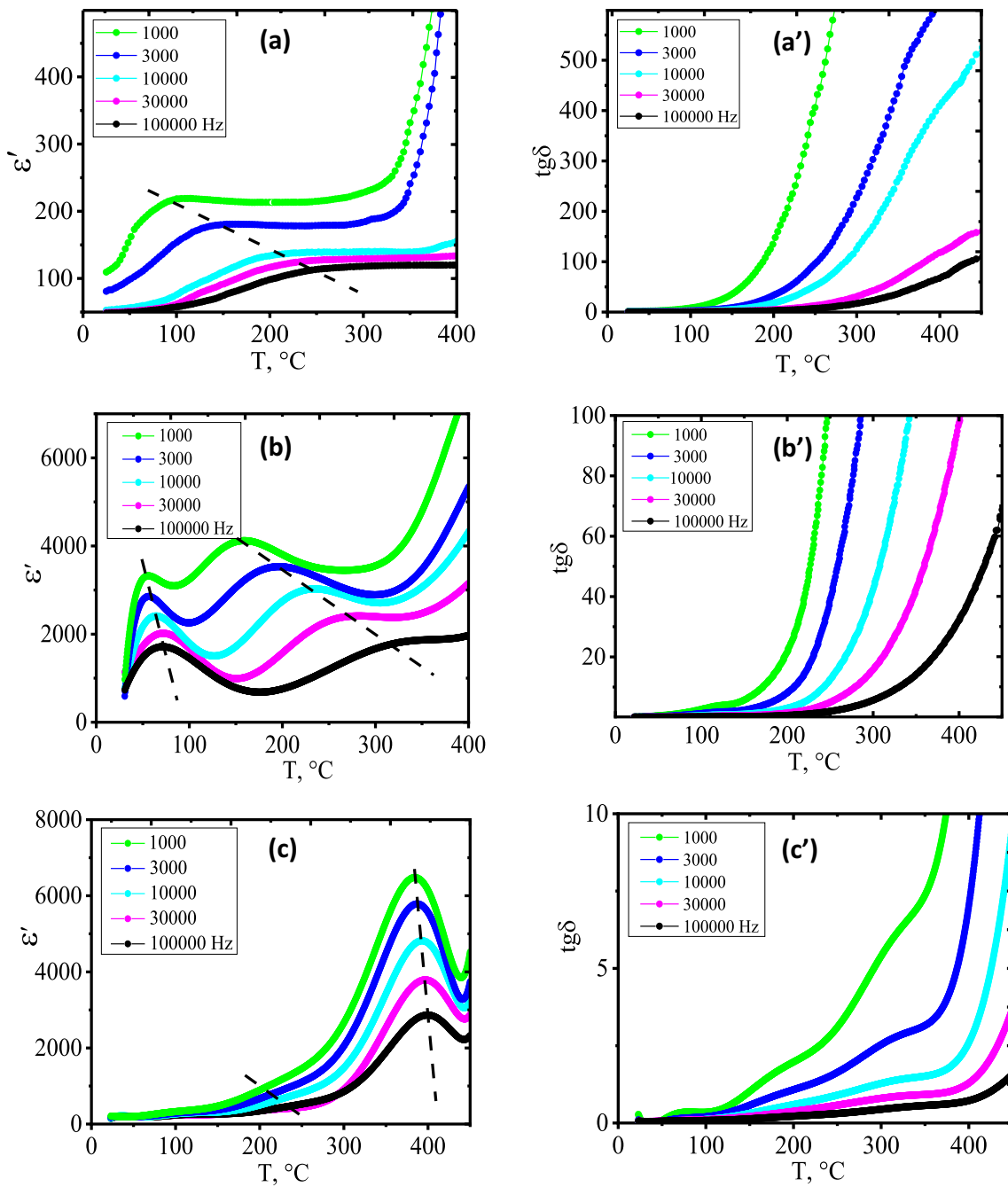
Fig. 5 The temperature dependencies of the real (**a,b,c**) of the dielectric constant of the PMnT and of the dielectric loss tgδ (**a′,b′,c′**) for $x = 0$, 0.4, 0.9 composites $(1-x)$PMnT–xPT

Based on the spectral shape of the reflection coefficient $R(\lambda)$ obtained at room temperature, the Kubelka−Munk (K−M) function was calculated, which is proportional to the ratio of the absorption coefficient α and the scattering coefficient s of an infinitely thick opaque sample [4, 20]:

$$F(R) = \frac{(1-R)^2}{2R} = \frac{\alpha}{s} \tag{1}$$

To estimate the bandgap, one can use the equation proposed by Tauc and Davis-Mott [21, 22]:

$$(h\nu \cdot \alpha)^{\frac{1}{n}} = A \cdot \left(h\nu - E_g\right) \qquad (2)$$

$$\left(h\nu \cdot F(R_\infty)\right)^2 = A \cdot \left(h\nu - E_g\right) \qquad (3)$$

where h is Planck's constant, ν—frequency, and A—proportionality coefficient. The value of the exponent n indicates the nature of the transition of the sample. It is known that $n = 1/2$ is for directly allowed transitions, and $n = 2$ is for indirectly allowed transitions. Substituting these quantities into E_g, (2) and analyzing the absorption edge, the interband transitions could be determined. For allowed direct transitions, the resulting reflection spectrum is converted to the K–M function.

Thus, the vertical axis is converted to the $F(R_\infty)$ value, which is proportional to the absorption coefficient. The proportionality coefficient A in the Tauc equation is replaced by $F(R_\infty)$. Then, the working equation is:

Further, using the K−M function $(h\nu \cdot F(R_\infty))^2$, the dependencies of $(E \cdot F(R_\infty))^2$ were built as functions from $h\nu$. The corresponding graphs are shown in Fig. 6. The point of intersection of the tangent to the straight sections with the abscissa determines the bandgap E_g. As can be seen from Fig. 6, the absorption patterns of the initial PMnT and 0.6PMnT–0.4PT composites are different.

The bandgap's energy values were calculated from the initial and doped ceramic samples' absorption spectra at room temperature, which is given in Table 1. It follows from Eq. (3) that there should be no quantum absorption indirect transitions with an energy lower than E_g. In this regard, the edge of fundamental absorption from the side of lower energies should be sharp. However, a detailed analysis of
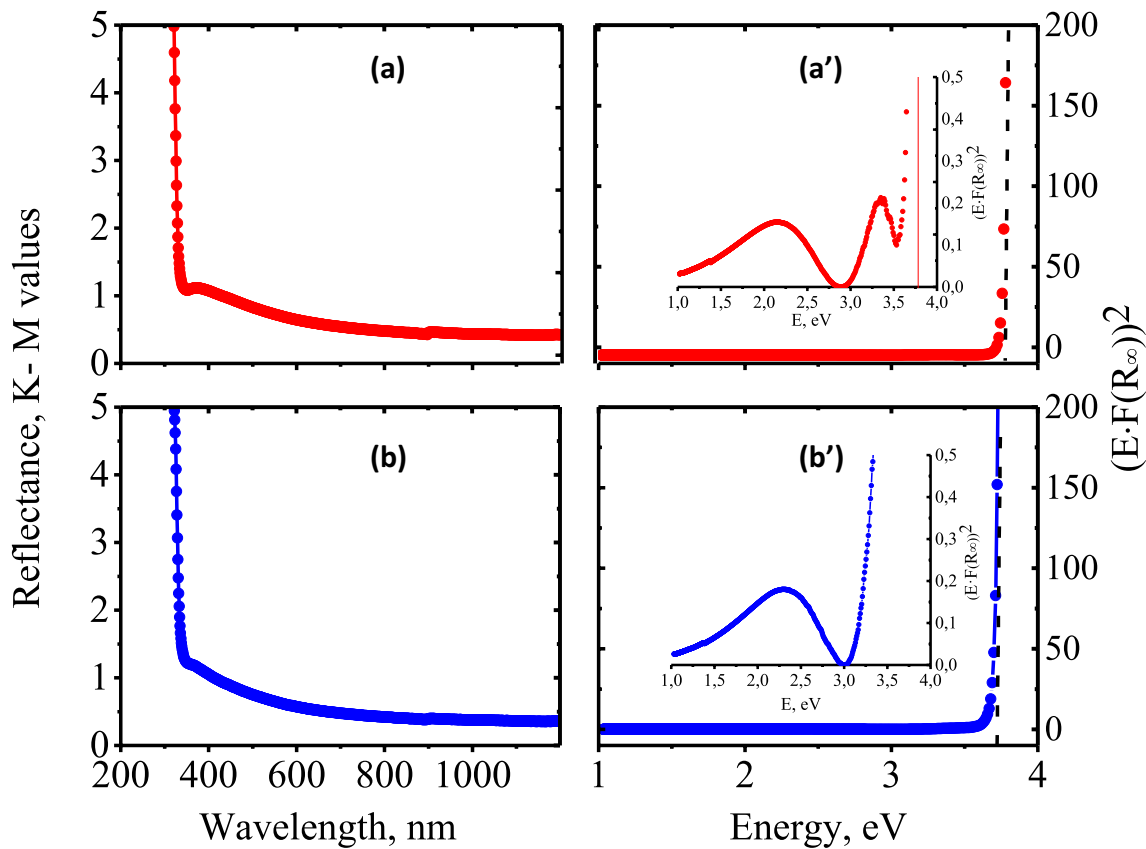
Fig. 6 The dependence of the absorption coefficient by Kubelka–Munk function on the wavelength and function $(E \cdot F(R_\infty))^2$ on the energy E of the composites PMnT (**a, a′**) and 0.6PMnT–0.4PT (**b,** **b′**). The insets on (**a′, b′**) show the enlarged parts of the spectrum corresponding to the absorption at $h\nu < E_g$

Table 1 The dependency of the energy bandgap E_g on the PT's mole fractions	PT's mole fractions	0	0.1	0.15	0.2	0.25	0.3	0.4
	E_g, eV	3.76	3.54	3.67	3.10	3.59	3.52	3.67

the dependency of $(E \cdot F(R_\infty))^2$ on $h\nu$ shows that the part of the spectrum to the left of E_g is actually nonlinear (see the insertions in Figs. 6a′, b′). Among the possible reasons for the nonlinearity of the dependency, the following can be singled out.

Since our composites are highly disordered and inhomogeneous and also have impurities, transitions between localized states lead to the nonlinear behavior of $(E \cdot F(R_\infty))^2$ in this region. Another reason could be the influence of random fields, the sources of which, as mentioned above, are randomly located electric dipoles. However, as can be seen from the insertion in Fig. 6a′, b′, after doped lead titanate into PMnT, the closest to E_g anomaly of the dependency of $(E \cdot F(R_\infty))^2$ on energy disappears. Nevertheless, as is known [16], doping of relaxors (lead titanate) suppresses the relaxor behavior of polarization and increases the degree of ordering. Hence, it follows a possible connection between the anomaly located to the left of E_g and at least one of the sources of ferroelectrics' relaxor behavior [23]. This anomaly corresponds, as seen from the insertion in Fig. 6a′, the energy value $E_i \approx 3$ eV. The results of calculating E_g for the range of $0 \leq x \leq 0.4$ of the dopant's mole fractions are shown in Table 1.

3.5 FTIR spectroscopy

FTIR spectra have been measured in isothermal transmission mode, and they show a broad intricate band in the $750-450$ cm^{-1} range, as shown in Fig. 7 for the composite 0.1PMnT–0.9PT.

The BO_6 octahedron of ferroelectrics of the ABO_3 perovskite family is characterized by four different types of vibrations: high-frequency stretching vibration, ν_1, low-frequency twisting, ν_2, bending, ν_3 and cation $-$ (BO_3), ν_4, vibrations. Only the $\nu_1 -$ ($B - O$) stretching vibrations fall

into the range our consideration. The given spectral range is sufficient for the analysis of stretching vibrations of perovskite structures of the ABO_3 type, and it is isolated from a wider spectral range. Similar spectra have been obtained for other composites studied in this work. We have not found a significant difference, except for the shift of the maxima of the vibrational components, and therefore they are not graphically presented here. Araújo et al. [24] demonstrated that it would be reasonable to divide such a complex band of the composites $(1 - x)PbMg_{1/3}Nn_{2/3}O_3 - xPbTiO_3$ into three vibrational components: stretching vibrations $\nu_1 -$ ($Mg - O$), $\nu_1 -$ ($Ti - O$), and $\nu_1 -$ ($Nb - O$). We also proceeded from the same considerations with Araújo et al. [24], and the band in the range of 750–450 cm^{-1} was approximated by three Lorentz functions. According to the maxima position of the stretching vibrations $\nu_1 -$ ($Mn - O$), $\nu_1 -$ ($Ti - O$), and $\nu_1 -$ ($Ta - O$), we plotted the graphs of the dependency of the dopant's mole fraction x on the wavenumber, in Fig. 7b. In the interval $0.2 \leq x \leq 0.6$, the graphs have a nonmonotonic behavior, while they change predictably outside this interval. Let us try to find out what the non-monotonic behavior of the graphs in this interval can be related to, for which we have to return to Fig. 4a, b . As it can be seen from Fig. 4a, in this interval, we observe a sufficiently sharp jump in the parameters of the tetragonal phase and a monotonic decrease in the parameters of the unit cells of the pyrochlore and pseudo-cubic phases. In the same interval, we observe a sharp increase in the pyrochlore phase concentration (see Fig. 4b). It should also be noted that of all the mole fractions studied in this work, and the maximum value of $\varepsilon'(T)$ was the composite 0.5PMnT–0.5PT, which was more than 8×10^3, and the relaxor behavior of the polarization of this composite was retained (Fig. 1S Supplemental data).

Thus, the reason for the nonmonotonic behavior of the components of stretching vibrations can be fluctuations in
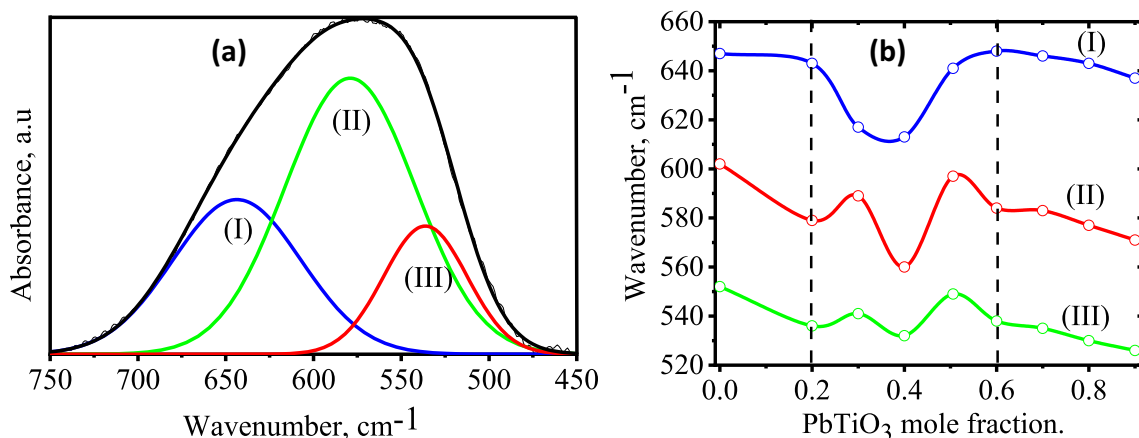
Fig. 7 FTIR spectrum of the composite 0.1PMnT–0.9PT with its deconvolution into fitting components I, II, and III (**a**). Positions of three components in FTIR spectra of composites $(1 - x)$PMnT–xPT as a function of x

the concentrations of the pyrochlore, pseudo-cubic phases, and a noticeable precipitation of the tetragonal phase.

3.6 Magnetic characteristic

Magnetic hysteresis loops for the samples with dopant's mole fractions at $x = 0$, 0.4, and 0.9, measured on a vibrating magnetometer, are shown in Fig. 8. We have found that the loops did not reach saturation even at $H = 2$ kOe.

The reason for the absence of the sample's magnetization' saturation is the presence of the magnetic pseudo-cubic phase, the pyrochlore phase with a sufficiently high concentration. As we already know, the pyrochlore phase consists entirely of non-magnetic ions. The ion Mn^{4+} has a smaller ionic radius ($r_1 = 0.053$ nm) compared to the ionic radius of Ta^{5+} ($r_2 = 0.064$ nm) [25, 26]. Therefore, it should be more favorable to form a crystal structure with Ta^{5+} ions instead of Mn^{4+} ions from the energy point of view. If not taken special technological measures, it would lead to the formation of the pyrochlore phase [27]. A small concentration of the perovskite pseudo-cubic phase present in the bulk of the sample forms weak hysteresis loops M(H). Doped lead titanate into PMnT most likely affects PMnT formation's thermodynamics but does not form a solid solution with it.

3.6.1 Magnetic capacity and magnetoresistance

Since the magnetic field affects the magnetic ordering, it indirectly changes the dielectric permittivity of magnetoelectric multiferroic materials. This effect is known as the magnetodielectric effect. However, as shown in [28], the large magnetodielectric effect can also be caused by magnetoresistance. And one of the prime causes of magnetoresistance
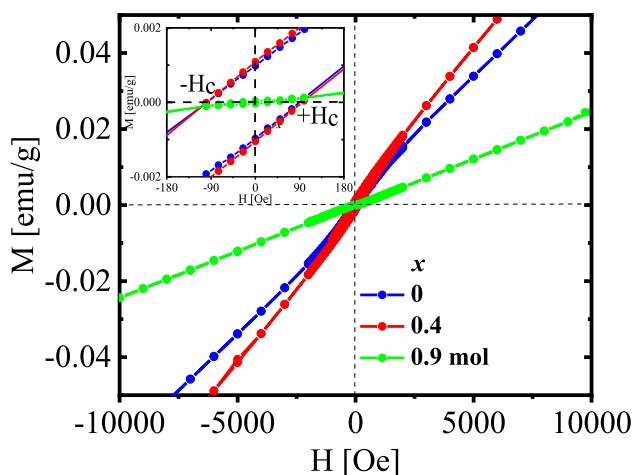
Fig. 8 The dependencies of magnetization on magnetic field for various dopant's mole fractions ($x = 0$, 0.4, 0.9) into the composites $(1-x)$ PMnT–xPT

is the heterogeneity of the studied samples. Each phase γ within the heterophase of the studied samples is corresponded to certain values of dielectric constant ε and conductivity σ. The difference of ε and σ in the near-electrode layer, the volumetric part of the phases, and grain-boundary layers can also be the cause of magnetoresistance.

It is known those heterogeneous systems can be described by the Maxwell–Wagner model, which is a set of series-connected flat capacitors, each of which corresponds to a certain phase with certain ε, tgδ, or γ. Each phase is limited by interlayer surfaces, which are characterized by Maxwell–Wagner polarization due to the accumulation of free charges on the interfaces. This, in turn, leads to dielectric dispersion and losses in the alternating electric fields, known as Maxwell–Wagner relaxation. The magneto-dielectric parameter (MD) was calculated using the formula:

$$MD(B) = \frac{\varepsilon'(B) - \varepsilon'(0)}{\varepsilon'(0)} \tag{4}$$

where ε′ is the real part of the permittivity, measured in an alternating electric field in the presence of a magnetic field and without it. The magnitude of the magnetic field $B = \mu\mu_0 H$ varied from 0 to 2 T.

All the measurements were carried out at room temperature in crossed electric and magnetic fields (E × B, E = electric, B = magnetic). Figure 9a–d shows the graphs of the MD(B) dependencies for the starting sample (Fig. 9a) and three different composites $(1-x)$PMnT–xPT. As seen in Fig. 9, the sign of MD(B) depends on the frequency of the alternating measuring electric field and the magnitude of the applied magnetic field. Common to all samples is the presence of the MD(B) dependencies in two sections. On the left section of each figure, a positive magnetoresistance is observed for three samples at the frequency of 500 Hz (see Fig. 9a, c, d). The positive magnetoresistance ends in the magnetic field range equal to 1580–1700 mT (approximately).

Measurements of MD(B) at frequencies of 100 kHz and 1 MHz show that before this range (1580–1700 mT) of the magnetic field, depending on the frequency of the measuring field, after a slight increase in weak magnetic fields, MD(B) does not change or have a negative sign. On the right section of each figure (Figs. 9a, c d)), a sharp increase in the amplitude of the negative MD was observed. Regardless of the frequency of the measuring field, a negative magnetodielectric effect is observed on the MD(B) dependency of the 0.3PMnT–0.7PT sample (Fig. 9b). It can be assumed that different mechanisms caused the MD(B) behavior in these two sections of the magnetic field.

Thus, it can be assumed that different mechanisms are responsible for MD(B)'s behavior in these two sections of the magnetic field.
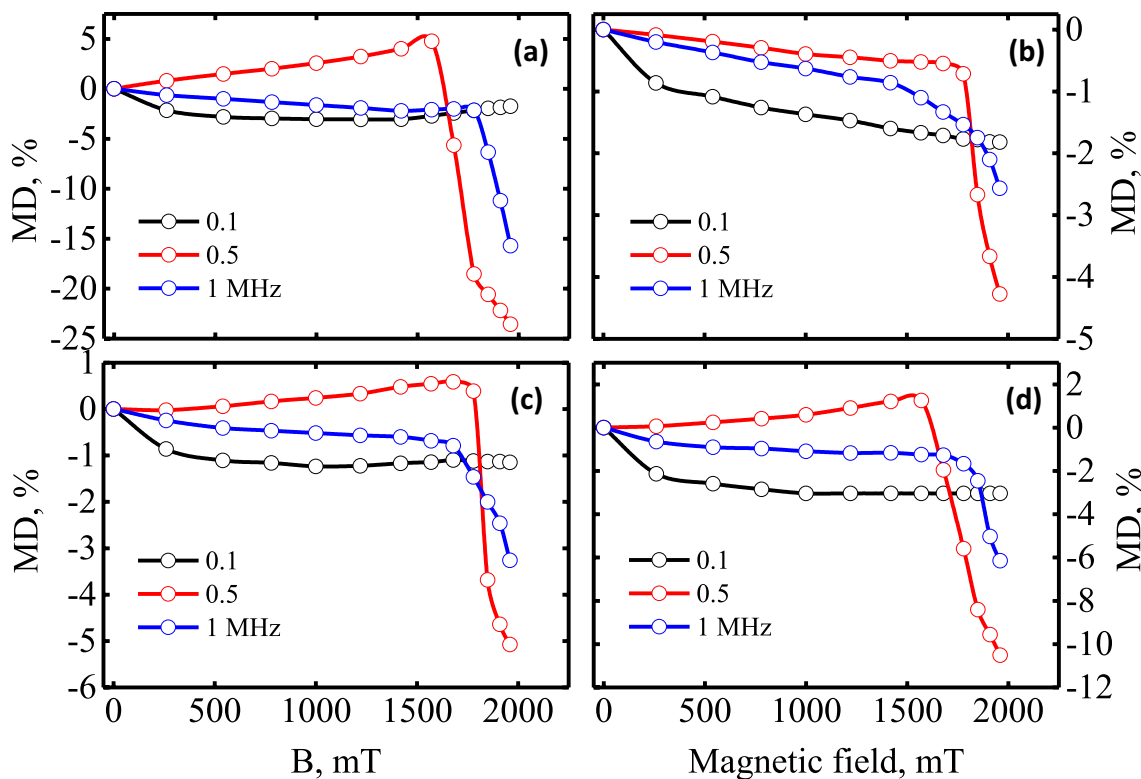
Fig. 9 The dependencies of the magnetodielectric effect's coefficient (MD) of the samples **a** PMnT, **b** composite 0.3PMnT–0.7PT, **c** 0.6PMnT–0.4PT, and **d** 0.9PMnT–0.1PT on the value of magnetic field induction
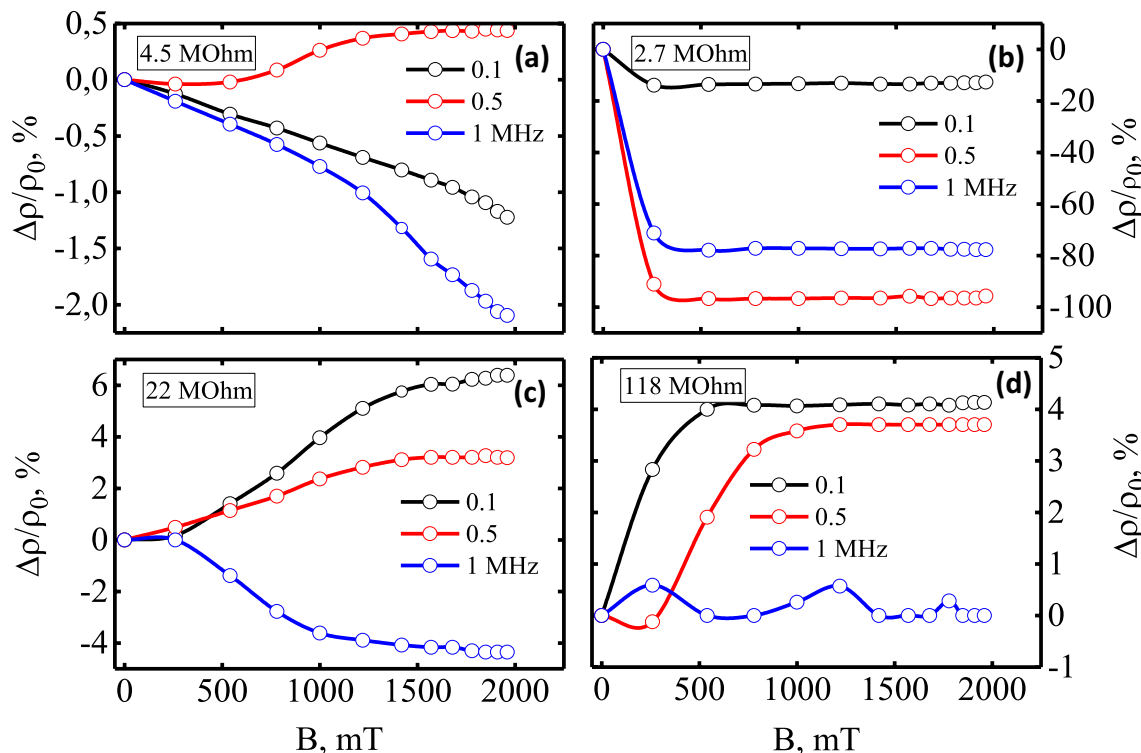
Fig. 10 The dependencies of the magnitude of the magnetoresistance of the starting sample **a** PMnT, **b** composite 0.3PMnT-0.7PT, **c** 0.6PMnT-0.4PT, and **d** 0.9PMnT–0.1PT on the magnitude of the magnetic induction

Further, we studied the dependencies of the resistivity $\rho(B)$ of the same samples on the magnitude of the magnetic field (Fig. 10 a, b). It should be noted that the samples at room temperature are good dielectrics; their DC resistance R was in the range $(2.7 - 118) \times 10^6$ Ω (see insets in Fig. 10). The generally accepted mechanism associated with the Lorentz force can be used to explain the positive magnetoresistance. The Lorentz force bends the path traversed by the conduction electron and lengthens it. This leads to an increase in the number of collisions of an electron with phonons and crystal lattice defects, as a result of which a positive magnetoresistance appears. This effect is common to all substances, and under normal conditions, it is not so significant. If the temperature does not change during measurements, then the expression for the magnetoresistance in weak fields (0.1–0.6 T) can be written as follows:

$$\frac{\Delta\rho}{\rho_0} = \frac{1}{24\text{n}^2 e}\left(\frac{B}{\rho_0}\right)^2 \tag{5}$$

where n is the concentration of electrons.

This expression is known as Kohler's rule [29]. In strong magnetic fields, the energy spectrum of the charge carrier changes drastically.

Negative magnetoresistance is a fundamental property of a crystal and is determined by the concentration of current carriers in it, the temperature and strength of the magnetic field, and in some cases, by the degree of impurity compensation.

To explain the negative magnetoresistance $\Delta\rho/\rho$, the model proposed in [30] can be used, according to which the quadratic dependency of the resistance reduction in a magnetic field is observed only in weak magnetic fields, after which the effect tends to saturation or passes into the region of positive magnetoresistance. The explanation for the resistance reduction of a crystal in a magnetic field is based on the concept of localization of electrons by an impurity atom, which can capture an extra electron and thereby acquire a magnetic moment (localized spin). Exchange interaction is possible between localized spins and conduction electrons. Since the interacting electrons' spins may not be parallel, then during scattering, the spin reorientation is also possible, i.e., along with the usual scattering mechanisms, an additional inelastic scattering mechanism appears. In an external magnetic field, the spins are oriented along the field. The number of spins oriented along the magnetic field B increases with the increase in the magnetic field.

Therefore, the inelastic scattering mechanism is partially turned off by the magnetic field, leading to a decrease in the crystal's resistance. With such a mechanism for changing the resistance in a magnetic field, the decrease in the magnitude should be proportional to the magnetization square. As a function of the magnetic field and temperature, follow the dependency:

$$\frac{\Delta\rho}{\rho_0} \propto N_M^2 B_j^2\left(\frac{B\mu^*}{k_B T}\right) \tag{6}$$

B_j is the Brillouin function, N_M—the localized spins' concentration, μ^*—the magnetic moment of the scattering center. This dependency is quadratic at small value B and saturates at $\mu^* B >> k_B T$.

As can be seen from the graphs shown in Fig. 10, for each sample, depending on the frequency of measuring field E, the curves show sections corresponding to the negative and positive effects of magnetoresistance, and some of which were saturated.

Since both positive and negative magnetoresistivity were observed during measurements, the experiment's magnetoresistance is the sum of two components: negative and positive.

Therefore, according to the dependency of the measuring field's frequency, the total magnetodielectric and magnetoresistive effects can be observed in the crossed field in the composites (1–x)PMnT–xPT and other multiphase objects.

4 Conclusions

The physical properties of the synthesized composites (1–x)PMnT–xPT have been studied. We found that the synthesis of the undoped PMnT in the air is always accompanied by the formation of pseudo-cubic perovskite $Pb_{0.70}Mn_{0.306}Ta_{0.66}O_{2.96}$ and pyrochlore phases $Pb_{1.94}Ta_2O_{6.94}$-$Pb_{1.96}Ta_2O_{6.96}$. The results show that the Maxwell–Wagner polarization is the main reason for the dielectric properties' relaxation behavior. The introduction of PT into PMnT as a doping component is accompanied by the suppression of the relaxation properties of (1–x)PMnT–xPT, which is one of the characteristics of many ferroelectromagnetic multiferroics. The doping lead titanate in PMnT results in a non-monotonic decrease in the bandgap E_g and a non-monotonic behavior of the stretching vibrations component in IR spectra, which can be caused by fluctuations in the concentrations of the pyrochlore and perovskite phases, as well as noticeable precipitation of the tetragonal phase. It has been discovered that positive and negative magnetodielectric and magnetoresistive effects are present in composites (1–x)PMnT–xPT at specific frequencies of the measuring field in a crossed electric and magnetic fields.

Declarations

Conflict of interest The authors declare that there is no conflict of interest.

References

1. A.P. Pyatakov, A.K. Zvezdin, Phys. Usp. **55**, 557 (2012)
2. K. Bhoi, H.S. Mohanty, Ravikant, M.F. Abdullah, D.K. Pradhan, S.N. Babu, A.K. Singh, P.N. Vishwakarma, A. Kumar, R. Thomas, D.K. Pradhan, Sci. Rep. **11**, 3149 (2021)
3. Y. Shimakawa, Y. Kubo, T. Manako, Nature **379**, 53 (1996)
4. B.K. Abdulvakhidov, K.G. Abdulvakhidov, A.P. Budnyk, S.A. Sadykov, T.A. Lastovina, M.A. Sirota, I.P. Dmitrienko, A.L. Bugaev, P.S. Plyaka, M.A. Vitchenko, I.V. Mardasowa, A.V. Soldatov, Mater. Res. Expr. **6**, 126319 (2019)
5. T. Kimura, T. Goto, H. Shintani, K. Ishizaka, T. Arima, Y. Tokura, Nature **426**, 55 (2003)
6. T. Lottermoser, T. Lonkai, U. Amann, D. Hohlwein, J. Ihringer, M. Fiebig, Nature **430**, 541 (2004)
7. M.D. Glinchuk, E.A. Eliseev, V.A. Stephanovich, B. Hilczer, Phys. Solid State **43**, 1299 (2001)
8. M.D. Glinchuk, V.A. Stephanovich, J. Phys. Condens. Matter **10**, 11081 (1998)
9. M.D. Glinchuk, V.A. Stephanovich, J. Appl. Phys. **85**, 1722 (1999)
10. W. Kraus, G. Nolze, J. Appl. Crystallogr. **29**, 301 (1996)
11. H. Yabuta, H. Tanaka, T. Furuta, T. Watanabe, M. Kubota, T. Matsuda, T. Ifuku, Y. Yoneda, Sci. Rep. **7**, 45842 (2017)
12. A.V. Pavlenko, A.V. Turik, L.A. Reznichenko, Y.S. Koshkid'ko, Phys. Solid State **56**, 1137 (2014)
13. X. Ding, G. Zhu, W. Geng, Q. Wang, Y. Wang, Inorg. Chem. **55**, 154 (2016)
14. F. Beech, W.M. Jordan, C.R.A. Catlow, A. Santoro, B.C.H. Steele, J. Solid State Chem. **77**, 322 (1988)
15. H.G. Scott, J. Solid State Chem. **43**, 131 (1982)
16. E.V. Colla, N.K. Yushin, D. Viehland, J. Appl. Phys. **83**, 3298 (1998)
17. S. Kamba, D. Nuzhnyy, S. Veljko, V. Bovtun, J. Petzelt, Y.L. Wang, N. Setter, J. Levoska, M. Tyunina, J. Macutkevic, J. Banys, J. Appl. Phys. **102**, 074106 (2007)
18. B.M. Vul, Uspekhi Fiz. Nauk **109**, 215 (1973)
19. V.A. Isupov, Tech. Phys. **42**, 1155 (1997)
20. G. Kortüm, W. Braun, G. Herzog, Angew. Chemie Int. Ed. Engl. **2**, 333 (1963)
21. J. Tauc, R. Grigorovici, A. Vancu, Phys. Status Solidi **15**, 627 (1966)
22. E.A. Davis, N.F. Mott, Philos. Mag. **22**, 0903 (1970)
23. M.P. Harmer, J. Chen, P. Peng, H.M. Chan, D.M. Smyth, Ferroelectrics **97**, 263 (1989)
24. E.B. Araújo, C.A. Guarany, K. Yukimitu, J.C.S. Moraes, A.C. Hernandes, Ferroelectrics **369**, 35 (2008)
25. A. Krichene, W. Boujelben, A. Cheikhrouhou, EPJ Web Conf. **29**, 00045 (2012)
26. M.C. Simoes, K.J. Hughes, D.B. Ingham, L. Ma, M. Pourkashanian, Inorg. Chem. **56**, 7566 (2017)
27. E. Aleshin, R. Roy, J. Am. Ceram. Soc. **45**, 18 (1962)
28. G. Catalan, Appl. Phys. Lett. **88**, 102902 (2006)
29. I.L. Spain, R.O. Dillon, Carbon N. Y. **14**, 23 (1976)
30. Y. Toyozawa, J. Phys. Soc. Jpn. **17**, 986 (1962)

Publisher's Note Springer Nature remains neutral with regard to jurisdictional claims in published maps and institutional affiliations.